Taylor & Francis
Taylor & Francis Group

Applied Artificial Intelligence
An International Journal

ISSN: (Print) (Online) Journal homepage: https://www.tandfonline.com/loi/uaai20

Assessment and Localization of Structural Damage in r/c Structures through Intelligent Seismic Signal Processing

E. Vrochidou, V. Bizergianidou, I. Andreadis & A. Elenas

To cite this article: E. Vrochidou, V. Bizergianidou, I. Andreadis & A. Elenas (2021) Assessment and Localization of Structural Damage in r/c Structures through Intelligent Seismic Signal Processing, Applied Artificial Intelligence, 35:9, 670-695, DOI: 10.1080/08839514.2021.1935589

To link to this article: https://doi.org/10.1080/08839514.2021.1935589

APPLIED ARTIFICIAL INTELLIGENCE
2021, VOL. 35, NO. 9, 670–695
https://doi.org/10.1080/08839514.2021.1935589

Taylor & Francis
Taylor & Francis Group

Assessment and Localization of Structural Damage in r/c Structures through Intelligent Seismic Signal Processing

E. Vrochidou [a], V. Bizergianidou[b], I. Andreadis[b], and A. Elenas[c]

[a]Department of Computer Science, International Hellenic University, Kavala, Greece; [b]Department of Electrical and Computer Engineering, Democritus University of Thrace, Xanthi, Greece; [c]Department of Civil Engineering, Democritus University of Thrace, Xanthi, Greece

ABSTRACT

In this work, a novel approach in post-earthquake structural damage estimation is investigated. The approach is formulated as a problem of both damage approximation and localization. The inter-story drift ratio and the global damage index of Park/Ang ($DI_{G,PA}$) are the estimated damage indicators for each floor of the structure. Artificial neural networks (ANNs), random forests (RFs), support vector machines (SVMs) with linear and radial basis function (RBF) kernels and adaptive neuro-fuzzy inference systems (ANFISs) are tested to predict the seismic damage state of each floor of an 8-storey reinforced concrete (r/c) building subjected to 155 natural and artificially generated seismic accelerograms. The damage potential of the accelerograms is described by three seismic parameters extracted from the response of the structure. The set of seismic accelerograms is defined by combining two outlier detection techniques, isolation forests and Z-score, while the set of seismic parameters is confirmed by minimum redundancy maximum relevance (mRMR) feature selection algorithm. Optimization methods are used to fine-tune the performance of all networks. Results indicate RFs and ANNs among the models with optimal performances, reaching average correct classification rates of up to 96.87% and 91.87% with RFs, and 96.25% and 90.12% with ANNs, for $DI_{G,PA}$ and ISDR, respectively.

ARTICLE HISTORY
Received 3 January 2021
Accepted 8 March 2021

Introduction

The ability of authorities to cope with natural disasters such as earthquakes directly depends on their ability to anticipate what will come next. For this reason, seismic vulnerability estimation on buildings is always on the forefront, emerged as the primer concern of earthquake engineering (Downey et al. 2018; Rus, Kilar, and Koren 2018). A detailed seismic performance assessment of urban buildings is essential for decision-making on post-earthquake crisis management, evacuation, repair, maintenance and reoccupation.

Various seismic damage assessment methods can be found in the literature (Ferreira, Mendes, and Silva 2019; Kappos 2016). Traditional statistical

CONTACT E. Vrochidou evrochid@cs.ihu.gr Department of Computer Science, International Hellenic University, Kavala, Greece

methods are not able, though, to deal with missing data or with noise in the data sample. Nonlinear data, such as seismic signal accelerograms, need models able to identify patterns and deal with nonlinear behaviors. Thus, intelligent models are widely used in the past few years for structural damage assessment due to their excellent learning capacity and their tolerance to inaccurate data. Inputs to intelligent models are descriptive features from which the models learn from in order to produce the desired output. In seismic damage assessment, the inputs usually refer to seismic parameters and the outputs to damage indices. Input parameters can either be seismic intensity parameters derived from the seismic excitations, or response-based parameters, extracted from response signals of the structure. Overall damage indices describe the post-earthquake status of buildings with a single value. maximum inter-storey drift ratio (MISDR) and the global damage index of Park/Ang ($DI_{G,PA}$) are two well-known effective descriptors of structural damage on buildings and are widely used as outputs of intelligent models toward damage assessment.

In Morfidis and Kostinakis (2017), a multilayer perceptron artificial neural networks (ANN) is tested for classifying structural damage based on MISDR using 14 seismic intensity parameters. The ANN is tested on 30 reinforced concrete (r/c) structures under 65 seismic excitations. Feature reduction also takes place, resulting in small values of mean square error (MSE), between 0.045 and 0.055 by using five seismic parameters. In Morfidis and Kostinakis (2018), the same authors use 18 input parameters, seismic and structural, as inputs to a multilayer feedforward perceptron ANN for MISDR classification. The ANN is tested for three configuration architectures reporting higher correct classification rate of 86.7% for a 3-storey building. In a more recent work (Morfidis and Kostinakis 2019), two ANNs are investigated for the same problem of seismic damage classification based on MISDR. The same earthquake dataset is used for the dynamic analysis of 90 r/c buildings. The ANNs inputs are 14 seismic intensity parameters. The final result is extracted after optimization of the networks' architecture, resulting in maximum correct classification rate of 93.9%. ANNs are also used in Hait, Sil, and Choudhury (2020) for the prediction of $DI_{G,PA}$ of r/c low-rise buildings under the excitation of seven pairs of natural ground motions. In Vrochidou et al. (2018), the performance of three intelligent models is studied; an ANN, a Mamdani-type fuzzy inference system (FIS) and a Sygeno-type FIS. A set of eight seismic intensity parameters derived from the dynamic analysis of an r/c frame model under 100 seismic excitations is used for MISDR estimation, resulting in up to 91% correct classification rate. In Tsiftzis, Andreadis, and Elenas (2006), a fuzzy scheme is introduced for structural and architectural damage classification based on MISDR value. A training set of natural accelerograms is used, and fuzzy representations of prototype signals are extracted to classify the unknown accelerograms through a fuzzy comparison with the prototypes.

Correct classification rates of up to 84% are reported. Three fuzzy pattern recognition models are tested in Andreadis, Tsiftzis, and Elenas (2007) to classify damage potential based on MISDR. A set of 400 accelerograms is used, and a set of 20 seismic intensity parameters is calculated for an r/c frame model. Classification rates of up to 85% are reported. A fine-tuned Mamdani-type FIS is trained in Vrochidou et al. (2016) to predict MISDR, resulting in 91% correct classification rate. The configuration includes a set of 100 seismic events and four seismic intensity parameters related to the damage occurred to an r/c model frame. An adaptive neuro-fuzzy inference system (ANFIS) is proposed in Elenas et al. (2013) for damage classification of both MISDR and $DI_{G,PA}$. Twenty well-known seismic intensity parameters are calculated from the nonlinear dynamic analysis of an r/c model under the excitation of a total set of 200 accelerograms, concluding to 90% correct classification rate.

All aforementioned approaches use seismic intensity parameters derived from the seismic excitation. However, response-based parameters, extracted from the response signals of the structure, are considered highly descriptive features that are sensitive to changes in structural parameters and external excitation (Huang et al. 2003; Masri et al. 2000). Response data is considered to mirror the dynamic characteristic of structures, such as natural frequencies, modal damping and modal shapes. In addition, the response of buildings is directly depended on the seismic ground excitation and its intensity parameters. Therefore, response-based parameters can also be used effectively for structural damage assessment. In Huang et al. (2003), an ANN is trained based on measured acceleration response data, while in Masri et al. (2000) a backpropagation neural network is trained to detect damages based on measured displacement, velocity and acceleration responses combined with input forces.

Moreover, in all above approaches, the estimated damage is the overall damage, and it refers to the entire post-earthquake building status. Targeted damage estimation separately on each floor of a building is relatively rare in the literature. Peak floor acceleration estimation of each floor of a structure is investigated in Lin and Lin (2020). Peak measurements of acceleration, velocity displacement, effective predominant period, integral of squared velocity and cumulative velocity are calculated from a vertical ground acceleration time-history. These parameters are the inputs to a support vector machine (SVM) for predicting peak floor acceleration on each floor. However, damage estimation is not direct, in terms of well-known damage indices, but it is based on the assumption that floor acceleration may cause structural damage. In another approach, Kubo et al. (2011) use servo-type accelerometers that are placed on specific floors of a high-rise building in order to estimate the intensity scale of earthquakes on the building floors out of three component of the seismic wave; east-west, north-south and up-down. Maximum acceleration and maximum velocity of each floor are used for the damage intensity

estimation. This work mainly focuses on the development of an early warning system and real-time seismic monitoring system, rather than on intelligent damage predictive models. Moreover, the proposed seismic intensity index is actually calculated directly from the measurements of the accelerometers, and it is not predicted from input parameters related to the damage index via machine learning.

This paper proposes a framework to predict accurately the structural damage on each floor of an r/c structure immediately after an earthquake. The proposed approach examines the response of the building separately on each floor toward damage estimation, classification and localization. Five intelligent models are tested; ANNs, RFs, SVMs with linear kernel, SVMs with RBF kernel and ANFISs. Optimization of all models takes place. Moreover, the velocity, displacement and acceleration response of each floor are considered for the seismic parameters' extraction. More specifically, for each floor, three seismic parameters and two damage indices, are calculated, under the excitation of 155 natural and artificially generated seismic signals. The initial sample of 200 accelerograms is optimized to 155 with a combination of two outlier techniques so as to exclude all samples that deviate from the dataset's normal behavior. The number of seismic parameters is also reduced from 18 to 3 with a feature selection technique so as to select the parameters with high correlation with the used damage indices and low correlation between themselves.

The proposed methodology contributes as follows: (1) classification and numerical assessment of two damage indices, MISDR and $DI_{G,PA}$ using five intelligent models, which have not been comparatively tested before in structural damage classification problems; (2) optimization of all models under the same configurations for objective comparative reasons; (3) ability, apart from estimation and classification, of localization of the damage among the floors of the examined structure; (4) use of highly descriptive seismic parameters extracted from the response of the structure, thus, of parameters directly related to the induced damage and the characteristics of the structure; (5) use of effective preprocessing techniques including data mining and feature selection; and (6) development of a generic methodology. The proposed strategy is tested to a specific r/c structure; however, it can be generalized to buildings with different structural characteristics. Experimental results indicate that it could provide an effective tool to serve for the purposes of rational decision making for disaster preparedness in three central ways: (i) for targeted humanitarian actions at the most affected buildings starting from the most damaged floors of the stricken areas;, (ii) for targeted maintenance/repair of the building focusing on where the greatest damages were detected and (iii) for the future design of more resilient buildings.

The rest of the paper is organized as follows. Firts section includes details regarding the dataset, the seismic parameters, the intelligent models and the examined structure. The next four sections deal with the configuration of each model, the optimization process and the obtained results. Comparative results, models' evaluation and discussion are presented subsequently. Last section concludes the paper.

Materials and Methods

The objective of the current section is a detailed account of the procedure that was followed and the means that were used in completing the experiments for the estimation of $DI_{L,PA}$ and ISDR. Details regarding the seismic excitations, the damage indices, the extracted parameters, the r/c structure and the intelligent models are included in this section. Moreover, configuration parameters of the models and formulation of the problem are described, where deemed necessary, in the following subsections.

Seismic Accelerograms

In total, 155 seismic accelerograms are used to test the proposed method; 100 natural and 55 artificially generated seismic signals. Natural accelerograms are acquired from the Pacific Earthquake Engineering Research Center (PEER) strong ground motion database (Berkley University of California 2020), which is reported as the largest database of processed, recorded ground motions. PEER strong ground motion database assures data processing consistency and accurate metadata retrieval; thus, it is widely used by engineers. Artificial accelerograms are generated according to the methodology proposed in Vrochidou et al. (2014). Artificially generated accelerograms are required, in order to test the seismic behavior of buildings under a wide range of seismic intensities where natural recordings cannot be found due to lack of nearby seismic station or due to low seismic activity at those regions. Thus, the final seismic accelerograms' dataset is formulated so as to cover all in-between values of the selected damage index for every floor of the examined building, giving the sufficient variety to the training process, and consequently, robustness to the final result.

The final data set of the 155 seismic accelerograms is defined after a data mining process, involving an initial dataset of 200 natural and artificially generated seismic accelerograms. This process is of great importance since in machine learning the quality of data is equivalent to the quality of the prediction or classification model.

Two outlier detection techniques are combined, the isolation forest (Liu, Ting, and Zhou 2008) and the Z-score (Rousseeuw and Hubert 2011). Isolation forest is an unsupervised learning algorithm based on the decision

tree algorithm. It isolates the outliers by randomly selecting a feature from the given set of features and then selects a split value between the maximum and minimum values of that feature randomly. Z-score is a parametric algorithm that indicates how many standard deviations a data point is from the sample's mean, assuming a Gaussian distribution. The excluded samples for both methods are those that display anomalous instances in the subsets based on ISDR for each floor. For both methods, when an outlier is detected on a floor, then the anomalous sample is excluded from the samples of all floors so as to have the same number of excitations for each floor. The final sample set of the 155 accelerograms results from the initial sample set with a subtraction of the outliers found.

Damage Index

Overall damage indices are the most commonly used response quantities able to describe the structural damage status of buildings within a single value. In this study, the ISDR and the $DI_{G,PA}$ are selected to express the induced seismic damage to each floor of the structure.

The ISDR index is defined as the difference of displacements at the adjacent two stories, normalized by the inter-story height (Yang, Pan, and Li 2010). $DI_{G,PA}$ is defined as the weighted average of the local damage indices of each element. The weighting function for each element is proportional to the energy dissipated in the element (Park and Ang 1985). Here $DI_{G,PA}$ is calculated separately for every floor of the examined structure.

ISDR and $DI_{G,PA}$ are global and deterministic, and they are considered reliable damage index of structural and nonstructural damage of r/c buildings. Depending on their numerical values, ISDR and $DI_{G,PA}$ are used to classify the damage potential in four classes, namely low (class 1), medium class 2), large (class 3) or total (class 4), according to the ranges provided in Table 1 (Vrochidou et al. 2018).

Parameters

The damage potential of a seismic accelerogram can be expressed through several seismic intensity parameters that are strongly related to the induced damage (Elenas and Meskouris 2001). In general, the damage of a structure is assessed from observed dynamic responses that derive by modifications in the modal parameters of the structure. The main concept is that the damage to

Table 1. Structural damage degree according to ISDR.

Low	Medium	Large	Total
≤0.5	0.5< ISDR≤1.5	1.5< ISDR≤2.5	>2.5
≤0.3	0.3< $DI_{G,PA}$ ≤0.6	0.6< $DI_{G,PA}$ ≤0.8	>0.8

a structure reduces its natural frequencies and changes its modal shapes. Therefore, features that derive from the response of structures under input excitations are directly related to the dynamic characteristics of the structure (Huang et al. 2003). Moreover, response-based parameters are strongly related to the seismic damage and can also be used for seismic damage evaluation (Ghobarah, Abou-Elfath, and Biddah 1999; Perrault and Guéguen 2015).

In this work six seismic parameters are calculated from the velocity, displacement and acceleration response signals, for every floor (or level) of the examined building, forming a final set of 18 parameters. The initial set, presented in Table 2, consists of parameters that are proved to be correlated with maximum ISDR and $DI_{G,PA}$ (Elenas and Meskouris 2001).

The first group of three parameters is calculated from the peak ground displacement/velocity/ acceleration (PGD/PGV/PGA) (Elenas and Meskouris 2001). PGA is the maximum amplitude of the ground acceleration time-history. PGV expresses the peak of the first integration of the acceleration record. PGD represents the maximum recorded displacement by second-order integration of the acceleration time history. Here, the same peak parameters are calculated from the three response signals on each floor of the examined building. Therefore, PGV is calculated as the peak inter-story velocity ratio (PIVR), PGD as the peak inter-story displacement ratio (PIDR) and PGA as the peak inter-story acceleration ratio (PIAR).

The second group of three parameters derives from the Arias intensity (I_A) (Arias 1970), defined by the equation:

$$I_A = \frac{\pi}{2g}\int_0^{t_e} [a(t)]^2 dt \tag{1}$$

where t_e is the total duration of the response signal and $a(t)$ is the response signal (displacement, velocity, acceleration) of every floor of the examined building. Thus, the three calculated parameters are the I_{Adis}, I_{Avel} and I_{Aacc}.

Three parameters are calculated from the destructiveness potential after Araya/Saragoni (DP_{AS}) as follows:

$$DP_{AS} = \frac{I_A}{v_0^2} \tag{2}$$

Table 2. Initial set of 18 seismic parameters.

Response signal		
Displacement	Velocity	Acceleration
PIDR	PIVR	PIAR
I_{Adis}	I_{Avel}	I_{Aacc}
DP_{ASdis}	DP_{ASvel}	DP_{ASacc}
CP_{dis}	CP_{vel}	CP_{acc}
$P_{0.90dis}$	$P_{0.90vel}$	$P_{0.90acc}$
CAD	CAV	CAA

where $v_0$is the intensity of zero-crossings and I_A is the Arias intensity. For the three different response signals, we calculate DP_{ASdis}, DP_{ASvel} and DP_{ASacc}.

The central period (CP) is defined as the reciprocal value of the number of positive zero-crossings of the seismic acceleration per time unit (Elenas et al. 2013). Here the CP is calculated for the displacement, velocity and acceleration response signals, deriving three parameters, CP_{dis}, CP_{vel} and CP_{acc}, respectively.

The power ($P_{0.90}$) [25] is a measure of the energy content of the seismic excitation per time unit, and it is defined as follows:

$$P_{0.90} = \frac{H_{0.95} - H_{0.05}}{T_{0.90}} \tag{3}$$

where $P_{0.90}$ is the power of seismic excitation, $H_{0.95}$ and $H_{0.05}$ are the energy levels at 95% and 5% of the Husid diagram (Husid 1969), respectively, and $T_{0.90}$ is the strong motion duration after Trifunac/Brandy (SMD_{TB}) (Trifunac and Brady 1978). SMD_{TB} is defined as the time elapsed between the 5% and 95% of the Husid diagram:

$$SMD_{TB} = T_{95} - T_{05} \tag{4}$$

Here, the $P_{0.90}$ is calculated for the displacement, velocity and acceleration response signals, deriving three parameters, $P_{0.90dis}$, $P_{0.90vel}$ and $P_{0.90acc}$, respectively.

The last three parameters are the cumulative absolute displacement/velocity/acceleration (CAD/ CAV/ CAA) calculated as

$$CAa = \int_0^{t_e} |a(t)|dt \tag{5}$$

where α(t) is the response signal (displacement/velocity/acceleration), and t_e is the total duration of the signal.

The minimum redundancy maximum relevance (mRMR) feature selection algorithm (Aghaeipoor and Javidi 2020) was applied to the set of the 18 extracted parameters, so as to identify the most correlated parameters with ISDR. ISDR is used as the reference damage index here and at the outlier detection method, due to the fact that it has a wider the value range compared to $DI_{G,PA}$, as it can be seen from Table 1, which makes its estimation a more demanding task. mRMR was applied in each floor to determine the parameters that were more correlated to ISDR and less related between them. The common results among all floors, were the three final selected parameters. These parameters are the PIDR, the CP_{dis} and the I_{Adis}, as shown in Table 3.

All final parameters are deriving from the displacement response signal, indicating the strong correlation between the damage on each floor with the displacement of the floor, something that is expected. Thus, the final sample

Table 3. Final set of three seismic parameters.

Displacement response signal		
PIDR	I_{Adis}	CP_{dis}

consists of 155 seismic signals for each level of the structure (floor), described by three parameters, while the induced damage degree is expressed with two damage indices. All numerical calculations in this work refer to a specific r/c frame model.

r/c Frame Building

The studied DI and all response signals refer to a specific two-dimensional mid-rise r/c frame model. The model simulates an 8-storey building with an eigenfrequency of 0.85 Hz. Details regarding the frame model can be found in Vrochidou et al. (2016). More specifically, the frame model is subjected to the 155 seismic excitations and a nonlinear dynamic analysis takes place, so as to calculate the ISDR and $DI_{G,PA}$, and the displacement response for every level of the frame. Although the methodology is applied to the specific frame, it can be generalized and can cover all possible building typologies. It is worth mentioning that all changes toward generalization refer only to the nonlinear dynamic analysis and not to the proposed methodology.

Intelligent Models

Five intelligent models are used here to verify the proposed methodology; an ANN, an RF, an SVM with linear kernel, an SVM with RBF kernel and an ANFIS. The models are used for both regression, i.e. estimating a numerical value for ISDR and $DI_{G,PA}$ for each floor, and classification, i.e. classifying the damage degree to one of the four categories provided in Table 1. The input of all models is the three parameters derived from the 155 seismic excitations for each of the eight floors of the examined building, and the output is the ISPR and $DI_{G,PA}$ damage indices estimation for each floor. All model architectures have been optimized. In the next sections, the configuration of the models, the fine-tuning process and the experimental results are presented in detail.

Artificial Neural Network (ANN)

The objective of this work is the development of a generic tool that once trained, it will be able to estimate the structural damage of a building immediately after an earthquake. The type on ANN selected in this work is a multilayer feedforward network (Hornik 1991). The model is trained separately for every floor. While training the model, we adopt a uniform

setting; for all damage categories, we use 70% of the seismic signal for training the network, 15% for testing and 15% for validation. For enhanced performance, the model's architecture is optimized via a genetic algorithm (GA) as follows.

GA Optimization of ANN

A GA is employed to define the optimal system's architecture, in terms of hidden layers and the number of neurons for every layer, so as to minimize the damage index prediction error.

The GA seeks for the optimal number of hidden layers, between one hidden layer, which is the most simplified network, and two hidden layers. The number of neurons of each layer is also defined through the GA, and it is selected to be up to 10 neurons. Thus, the GA seeks the optimal architecture between one or two hidden layers of up to 10 neurons each. Limitations are set so as not to increase the complexity of the network and therefore the computation burden and execution time. Three parameters are therefore used $x = [x_1, x_2, x_3]$; one for the number of hidden layers (x_1), one for the number of neurons of the first layer (x_2) and one of the number of neurons of the second layer (x_3). Each parameter is a gene, and each genes' combination is a chromosome. The performance of each gene is evaluated by a fitness function. The lower the value of the fitness function, the strongest the gene and, thus, the stronger the possibility to survive on the next generation. The fitness function in this work is the mean square error (MSE) between the calculated and estimated value of the examined damage index, derived by the testing and validation set, from five ANNs. More specifically, the ANN is executed five times toward statistical independence and robustness, so as to eliminate any random false positive estimations, and returns as output the average of their MSEs.

$$FitnessFunc. = \frac{\sum_{i=1}^{i=5} MSE(testandvalidation)}{5} \tag{6}$$

$$MSE = \frac{1}{n}\sum_{i=1}^{n} |(target - output)|^2 \tag{7}$$

where n is the sample size.

The GA needs to cope with the following limitations:

- The number of generations. Here, the GA is set to run for 100 generations.
- Stall generation and function tolerance. Here, for each generation, the maximum population is set to 100 genes' combinations and function tolerance is set to 10^{-6}.

Table 4. GA results for ANN's optimization on every level.

	GA final result			
Level	x_1	x_2	x_3	No. of appearances
Level 1	2	4	5	84
Level 2	2	6	8	22
Level 3	2	9	7	43
Level 4	1	7	0	100
Level 5	2	7	10	49
Level 6	2	6	3	22
Level 7	**1**	**2**	**0**	**60**
Level 8	2	9	7	30

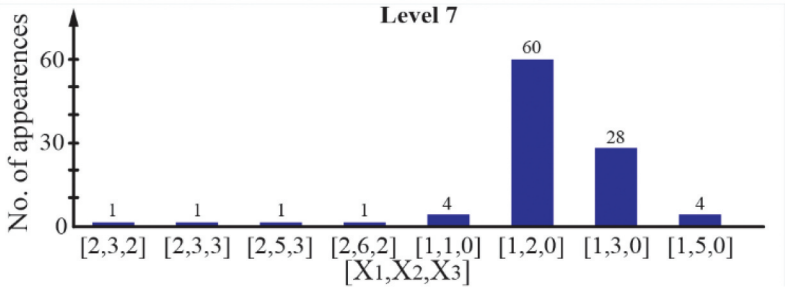

Figure 1. Histogram of GA results for ANNs optimization for 100 generations on level 7.

Additionally, an output function has been added so as to return the optimal result for every generation. When the GA finishes, the final result of the GA is compared to the results of each generation. The result of the final selected architecture is the combination that appears most times, i.e., on most generations, for each floor. This is to eliminate any coincidental results. GA results are summarized in Table 4.

In Figure 1 is presented the histogram of the GA results on the seventh floor, also marked in bold in Table 4. The bins in the figure represent all possible GA parameter combinations, while the bin heights represent the number of appearances of each combination in 100 generations. In the illustrated example of Figure 1, the most frequent combination, having 60 appearances, is x = [1, 2, 0], as also shown in Table 4. In all cases, the final GA architecture coincided with the most appearing architecture over the generations. Here, once again the ISDR is selected as the damage index for the configuration of the GA as the output of the model, due to its wider range of values.

Random Forest (RF)

The second proposed model is an RF. RFs are less computationally expensive than ANNs, do not require a GPU for training and are tolerant of overfitting since the model reduces high variance by combining many decision trees into

one ensemble architecture (Lei et al. 2020). In the RF approach, each tree is trained with 63.2% of the samples. RF here is used for regression. The predictor variable m is the number of all predictions divided by three. This value does not change. The rest of the data, 36.8%, are used for the out-of-bag error rate (OOB). In this work, the RF is optimized via a GA, as described in the next subsection.

GA Optimization of RF

A GA algorithm is used for the optimization of the minimum size per leaf ($x = [x_1]$) of the RF model, i.e. the minimum number of observations per leaf. The leaf is the final node of a decision tree, and the observations are the samples that ended up on the leaf. This parameter affects the depth of the decision tree because it forces it to grow until it achieves a goal. In the RF algorithm, the random selection of its training observations and variables, gives it the freedom to grow as required, without applying pruning to avoid overfitting.

Here, the optimal value of the minimum leaf size is indicated by the GA, between a minimum value, set to 2, and a maximum value, set to 20. This range was selected after a trial-and-error process, in order for the decision trees to develop sufficiently since our sample size are 155 seismic signals. Applying the selected range, the observations per leaf will be between 2 to 20. The algorithm will develop 100 such trees for the creation of the RF. In this application, gene and chromosome is the variable defined from the minimum leaf size. The performance of the chromosome is evaluated from the fitness function defined in Equation (8). The lower the value of the fitness function, the stronger the chromosome, thus, the bigger the possibility for it to continue to the next generation.

The RF is executed five times within the fitness function and returns the average of the MSEs of five random RFs, exactly as implemented at the ANN's optimization, according to Equation (7).

$$FitnessFunc. = \frac{\sum_{i=1}^{i=5} MSE(out - of - bag)}{5} \tag{8}$$

The GA terminates when either of the following criteria is fulfilled:

- The GA is set to run for 100 generations. At each generation, the population is set to 100 chromosomes.
- The fitness tolerance, i.e. the average error between generations, to be less or equal to 10^{-6}.

An output function is also used in the RF optimization process, that returns the best result of each generation. The final outcome of the GA is compared to the most appearing result for all generations. The result that is applied to

Table 5. GA results for RF's optimization on every level.

	GA final result	
Level	x_1	No. of appearances
Level 1	**2**	**47**
Level 2	2	44
Level 3	2	31
Level 4	2	53
Level 5	2	41
Level 6	2	39
Level 7	2	68
Level 8	2	41

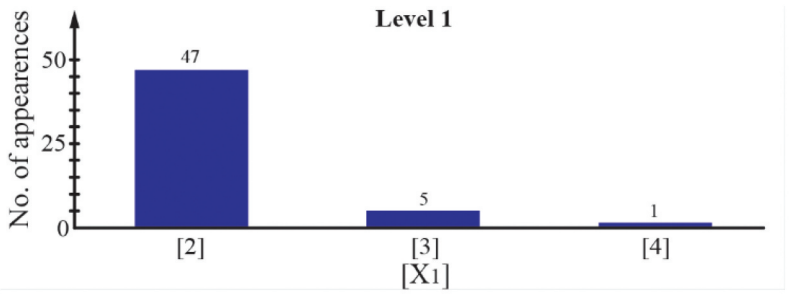

Figure 2. Histogram of GA results for RFs optimization for 100 generations on level 1.

optimize the RF is the one that appears most times, exactly as in the ANN's optimization process. Table 5 summarizes the GA results for the minimum leaf size, on every floor.

In Figure 2 is presented the histogram of the GA results on the first floor, also marked in bold in Table 5. The bins in the figure represent all possible GA parameter combinations, while the bin heights represent the number of appearances of each combination in all generations. In the illustrated example of Figure 2, the most appearing value is the value 2, having 47 appearances, then value 3 with 5 appearances and value 4 with one appearance. Thus, the most common result among the generation is x = [2], as reported in Table 6 and as it can be observed in the figure.

The total number of generations in this example equals 53, meaning that the GA ended due to fitness tolerance thresholding before reaching the limit of 100 generations.

Table 6. Grid search optimization result for SVMs on every level, for linear and RBF kernel.

	Linear Kernel			RBF Kernel		
Levels	C	ε	No. of appear.	C	ε	No. of appear.
Level 1	1	0.1	27	3	0.1	36
Level 2	1	0.1	92	3	0.1	30
Level 3	**1**	**0.1**	**82**	25	0.1	47
Level 4	1	0.2	15	3	0.1	35
Level 5	1	0.1	75	25	0.1	27
Level 6	1	0.1	91	25	0.1	25
Level 7	25	0.3	11	3	0.2	17
Level 8	1	0.1	57	2	0.1	56

Support Vector Machine (SVM)

SVMs (Cherkassky and Ma 2004) can be used for regression, maintaining all the main features that characterize the algorithm e.g. the maximal margin. It can solve linear and nonlinear problems based on a simple idea: SVM creates a line or a hyperplane which separates the data into classes. Here, the problem of optimal parameter selection for the SVM-regression construction algorithm is the problem of $x = [C, \varepsilon]$ minimization. C is the regularization parameter and ε is the error sensitivity parameter.

Parameter C determines the exchange between the model complexity and the degree to which deviations greater than ε are tolerated in optimization. Parameter ε adjusts the width of the ε-insensitive zone, which is used to fit the training data. The value of ε can affect the number of support vectors needed to create the regression function. Both parameters C and ε can affect the model's complexity (Nguyen and de la Torre 2010).

Grid Search Optimization of SVM

Here, the Grid search algorithm (Huang, Mao, and Liu 2012) is used for the optimization of parameters C and ε. The optimization problem is solved for two kernels; linear and RBF. The possible parameter values for C and ε were

C: [1, 2, 3, 4, 5, 6, 7, 8, 9, 10, 15, 20, 25]

ε: [0.1, 0.2, 0.3, 0.4, 0.5]

Grid search algorithm examines all possible combinations and returns the one that displays minimum MSE. The process was repeated 100 times to confirm the optimal combination, as the combination that prevailed in most of the trials. The optimal combination is subsequently used for training the SVM models.

The process is implemented for each floor of the structure for both kernels, linear and RBF. Optimization results are summarized in Table 6.

A very small value of parameter C will cause the optimizer to look for a larger-margin separating hyperplane, even if it results in more misclassified points. Big values of C refer to smaller tolerance to errors. The value of parameter ε defines a margin of tolerance where no penalty is given to errors. The larger the ε, the larger the errors one admits in the solution. The value of ε is small to all levels, equal to 0.1, for both kernels, however at the levels with class 4 damages, (Levels 1, 4 and 7) the value of ε is greater (0.2 and 0.3).

For the SVM with a linear kernel, the value of C is also big at levels 7 that display the greater damages. This can be explained due to the fact that damage indices of class 4 display a wide range of values, due to lack of upper limits in class 4, thus, in order to follow the linear distribution, bigger margins are required. Figure 3 illustrates the histogram of grid search optimization results for SVMs with linear kernel for 100 repetitions on the third floor, also marked

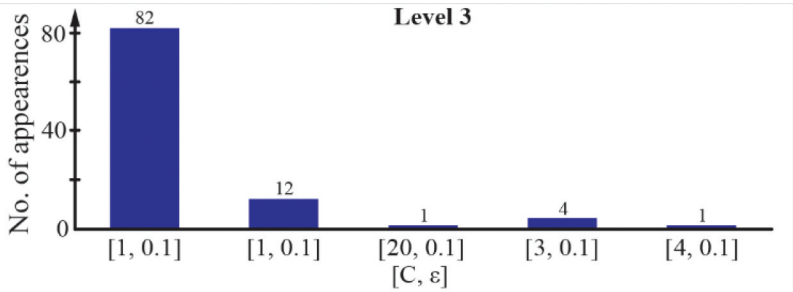

Figure 3. Histogram of grid search optimization results for SVMs with linear kernel for 100 trials on level 3.

in bold in Table 6. The most frequently occurred combination is the [*C*, *ε*] = [1, 0.1] with 82 appearances out of 100 trials. At levels with bigger damages, due to bigger value fluctuations thus more difficult prediction, the combinations of *C* and *ε* parameters vary. For this reason, the most appearing combination has a low value. On the other hand, on floors with smaller damages, fewer parameter combinations appear, displaying bigger number of appearances.

Adaptive Neuro-fuzzy Inference System (ANFIS)

ANFIS is widely used to produce nonlinear models of procedures so as to determine input–output relationships. In the recent years, efforts are made to find the optimal values of modeling parameters in order to decline training error and increase modeling accuracy. The GA-ANFIS model is used to minimize the prediction error during training and testing of the network (Begic Fazlic, Avdagic, and Omanovic 2015).

GA-ANFIS uses two parameter types that need training; the parameters at the fuzzification layer and the parameters at the last layer of ANFIS. More specifically, nine the three seismic parameters are used as inputs to the ANFIS for the first level of fuzzy model optimization. After that, they are used as inputs in the GA for the second level of fuzzy model optimization within GA-ANFIS system. Thus, GA-ANFIS performs optimization in two steps. The parameters that are updated from the GA are the parameters of membership functions (MFs) at the fuzzification layer, for Gaussian MFs.

GA Optimization of ANFIS

According to the above, the MFs are Gaussian functions. The MF parameters are randomly initialized on the first step, and then they are updated from the GA based on the performance of the ANFIS. When the MSE is less than a predetermined threshold, in our case, lower than 10^{-5}, the GA stops the

optimization of the ANFIS parameters. When the threshold criterion is not met, the GA stops after 100 iterations.

Comparative Results and Discussion

In this section, the results of all approaches are presented, compared and discussed. All data regarding classification rates and MSE for all models per floor are included in Table 7 for ISDR, and in Table 8 for $DI_{G,PA}$, respectively. The last line on each table provides the average MSE and classification rate of the model for all floors. All networks have been tested 100 times for statistical reasons in order to achieve convergence. Thus, the MSE provided in all consequent tables refers to the average result of 100 trials.

In order to translate the experimental results, first, we need to underline that the two selected damage indices differ significantly in value ranges (Table 1). This is more obvious in Table 9, where a statistical investigation of the damage values is presented; for both indices, the minimum, maximum, mean and median numerical values have been recorded. The maximum value for $DI_{G,PA}$ appears at level 7 and is equal to 0.93, while for ISDR the maximum value is also at level 7 and is equal to 6.93. These values are marked in bold font in the table. Narrow value ranges, thus smaller

Table 7. Aggregated results for ISDR estimation of all optimized models, per level and in total.

	ISDR									
	RF		**ANN**		**GA-ANFIS**		**SVM linear**		**SVM RBF**	
Levels	**MSE**	**Class.**	**MSE**	**Class.**	**MSE**	**Class.**	**MSE**	**Class.**	**MSE**	**Class.**
Level 1	9.82E-02	84%	9.91E-02	76%	2.09E-01	69%	1.28E-01	57%	1.56E-01	54%
Level 2	5.2 E-03	95%	5.50E-03	95%	2.90E-02	95%	7.80E-03	92%	6.40E-03	94%
Level 3	3.40E-03	96%	2.10E-03	96%	2.43E-02	91%	5.60E-03	95%	4.30E-03	92%
Level 4	1.02E-01	93%	1.97E-02	94%	2.40E-01	87%	6.63E-02	71%	1.16E-01	81%
Level 5	8.50E-03	94%	6.90E-03	95%	6.84E-02	88%	1.23E-02	86%	1.08E-02	83%
Level 6	5.00E-03	96%	4.70E-03	97%	6.80E-03	95%	8.70E-03	95%	6.80E-03	95%
Level 7	2.91E-01	87%	2.87E-01	76%	4.31E-01	64%	4.19E-01	37%	5.23E-01	43%
Level 8	2.70E-03	90%	2.50E-03	92%	7.30E-03	89%	4.50E-03	85%	4.40E-03	84%
ALL	6.46E-02	91.87%	5.35E-02	90.12%	1.27E-01	84.75%	8.16E-02	77.25%	1.03E-01	78.25%

Table 8. Aggregated results for $DI_{G,PA}$ estimation of all optimized models, per level and in total.

	$DI_{G,PA}$									
	RF		**ANN**		**GA-ANFIS**		**SVM linear**		**SVM RBF**	
Levels	**MSE**	**Class.**	**MSE**	**Class.**	**MSE**	**Class.**	**MSE**	**Class.**	**MSE**	**Class.**
Level 1	3.15E-03	96%	2.73E-03	94%	2.85E-02	90%	3.90E-03	94%	8.76E-03	95%
Level 2	2.99E-06	100%	3.76E-06	100%	1.43E-05	100%	6.36E-05	100%	6.36E-05	100%
Level 3	1.08E-06	100%	8.97E-07	100%	9.85E-06	100%	1.25E-05	100%	1.25E-05	100%
Level 4	9.11E-04	99%	3.89E-04	100%	3.23E-02	93%	7.39E-03	99%	8.21E-03	99%
Level 5	2.81E-05	100%	2.72E-05	100%	3.62E-04	100%	1.35E-04	100%	1.35E-04	100%
Level 6	4.48E-06	100%	5.36E-06	100%	1.37E-04	100%	2.57E-05	100%	2.57E-05	100%
Level 7	8.93E-03	80%	1.07E-02	76%	2.99E-02	69%	4.92E-02	54%	1.41E-02	82%
Level 8	6.89E-07	100%	6.98E-07	100%	3.86E-06	100%	3.16E-06	100%	3.16E-06	100%
ALL	1.69E-03	96.87%	1.73E-03	96.25%	1.14E-02	94%	7.59E-03	93.37%	3.91E-03	97%

Table 9. Maximum, minimum, mean and median prediction values for both damage indices per floor with optimized ANNs.

	$DI_{G,PA}$				ISDR			
Levels	Min.	Max.	Mean	Median	Min.	Max.	Mean	Median
Level 1	0.0000	0.7439	0.0881	0.0532	0.0000	5.0000	1.0183	0.7400
Level 2	0.0000	0.0209	0.0026	0.0018	0.0000	1.3400	0.5508	0.5700
Level 3	0.0000	0.0097	0.0018	0.0014	0.0000	1.0500	0.4960	0.5400
Level 4	0.0000	0.3594	0.0210	0.0122	0.0000	5.1500	0.8091	0.7600
Level 5	0.0000	0.0369	0.0105	0.0098	0.0000	1.5300	0.6885	0.7300
Level 6	0.0000	0.0160	0.0043	0.0039	0.0000	1.0800	0.5596	0.6300
Level 7	0.0000	**0.9357**	0.1389	0.0709	0.0000	**6.9300**	1.7559	1.4800
Level 8	0.0000	0.0048	0.0009	0.0007	0.0000	0.8000	0.4259	0.4700

fluctuations, result in optimal prediction results for $DI_{G,PA}$. This is the main reason why ISDR is the selected reference damage index in all optimization techniques throughout this work, i.e. toward optimizing its, comparative to $DI_{G,PA}$, poorer performance. Table 9 reveals that for the examined structures damages of class 3 and 4 mainly occur at levels 1, 4 and 7. These floors are also the ones with maximum MSE and lower correct classification rates for all models, as seen in Tables 7 and 8.

Maximum MSE is due to the lack of upper limit on damage class 4 (Table 1), providing a wider range for ISDR and $DI_{G,PA}$ estimation values and thus bigger MSEs. A damage estimation that may exceed in value, would still refer to damage class 4. Thus, even though damage classification is correct, it returns a big MSE value. In this case, MSE should not be evaluated. Moreover, class 4 refers to total damage/collapse of the building. Therefore, in case of class 4, MSE plays an insignificant role, and the prediction is considered successful as long as the damage is attributed to the correct class (class 4) regardless of the exact estimated damage index value. Additionally, when class 4 is correctly estimated in one level, referring to total collapse, then the results on all other levers should not be taken into consideration in the overall evaluation.

Lower classification rates are attributed to the way the data sample is divided into the four damage categories

In order to better understand why damage estimation is more difficult to the most damaged floors, we have to look in detail how the sample is divided into the four categories. Table 10 presents the distribution of the samples in the four damage categories for ISDR. We present this distribution for ISDR as it is the most difficult damage index to be predicted due to its big value range. However, for $DI_{G,PA}$, the distribution of samples is almost the same as for ISDR.

From Table 10, we can see that the sample displays large or total damage values only on levels 1, 4 and 7. Moreover, almost the same number of samples for all damage categories is only provided on level 7. In Table 10 are also summarized statistical features of the samples according to their distribution

Table 10. Sample distribution on floors according to ISDR.

	Damage class					
Levels	1 low	2 medium	3 large	4 total	Max.	Dev.
Level 1	55	68	19	13	5	0.87
Level 2	65	90	0	0	1.34	0.09
Level 3	72	83	0	0	1.05	0.06
Level 4	55	87	11	2	5.15	0.44
Level 5	56	97	2	0	1.53	0.15
Level 6	61	94	0	0	1.08	0.07
Level 7	**40**	**39**	**39**	**37**	**6.93**	**2.45**
Level 8	89	66	0	0	0.80	0.03

per floor; maximum value and deviation. In level 7, it is reported the maximum ISDR value and a maximum deviation of values. The deviation is related to the big value range of damage class 4 as it is already mentioned; large deviation indicates that values of the same class may be far apart and that there may be large fluctuations between values, that consequently affects the estimation performance of the models.

This fact can be better observed in Figure 4, where the sorted ISDR values per floor are presented. From Figure 4, it is obvious that floors with greater damages are the ones with the wider ISDR value range and with the most abrupt changes between values. Thus, estimating those values is more challenging.

A potential solution would be the augmentation of samples in all floors in a way to enrich all in-between ISDR values that are missing. In this way, all damage classes would be equally managed by the prediction models. Future work could include more data samples and the reduction of ISDR deviation to the most damaged levels. Data augmentation for training for both damage indices could enhance the performance of the models, especially in the most vulnerable floors.

Next, based on the above, the performance of each model is evaluated. The optimized ANNs, as defined in Table 4, are tested for each floor. Tables 7 and 8 include numerical results per floor for both damage indices for the optimized ANNs. ANNs, in general, require more data in order to actually be effective. The optimized RF models are configured according to the results presented in Table 5 and are tested for each floor. Results here, as for the ANNs reveal the greater damages on floors 1, 4 and 7, are having the most difficulty in being predicted accurately. At the most damaged levels, the total MSE appears to be higher compared to the rest levels, and classification rates are lower compared to the rest levels. This a general observation, for both damage indices and it is attributed to the wide range of values of class 4 for both damage indices, as already explained. However, $DI_{G,PA}$ displays better prediction results than ISDR, due to the narrower value ranges with smaller fluctuations. The optimized SVM models as shown in Table 6, are tested for every floor. The process is the same here as for all models, for both SVM

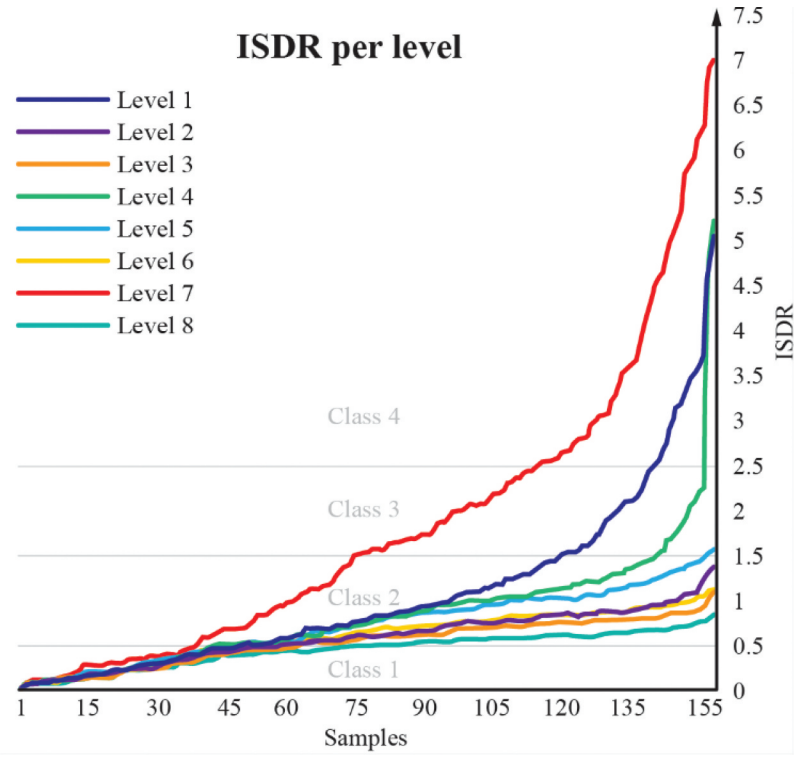

Figure 4. Sorted ISDR sample values per level.

linear and RBF kernel. Results on Tables 7 and 8 reveal that the model fails to predict the damage indices efficiently on the levels of class damage 4, especially on the seventh floor. Correct classification rates are low, and the MSE is relatively big, compared to other floors. The variety of parameters combinations derived from the Grid Search algorithm on the levels of damage class 4 indicate that maybe another parameter combination may have been more effective than the most appearing combination, which prevailed in appearances number from other combinations by very little. Tables 7 and 8 also include numerical results of the RBF SVM. Numerical results indicate that optimized SVM with RBF kernel did not outperform any of the previously presented models. More specifically, in levels 1 and 7, classification rates are lower compared to previous models. However, the SVM with RBF kernel exhibits a slightly better classification performance compared to SVM with linear kernel, as it can be seen from the two comparative tables. In general, $DI_{G,PA}$ displays better estimation performance than ISDR, for all models so far. The evaluation of the GA-ANFIS is in line with all previously presented models. Numerical results indicate, once again, low classification performances and large MSEs to the levels with seismic damage of class 4. The $DI_{G,PA}$ results to better performances compared to ISDR, as in all previous model architectures

In a first observation between all models, RF provides better estimation performances for both damage indices. The second better performance comes from the ANN. However, both performances are very close, even though these two models are based on different architectures. ANNs are organized in layers that include interconnected nodes with an activation function that computes the output of the model. RFs are ensemble decision trees where the final leaf node is the average class. The main advantage of RFs over ANNs is that they combine predictions of many decision trees into one model and are less prone to overfitting. RFs are less computationally expensive, while ANNs require much more data to be equally effective. RF is easier to customization, since the development of many trees aims for better adaptation of the algorithm to the problem. ANNs architecture, on the other hand, is the most important aspect affecting the final results. SVMs with both kernels provided medium performances. This is attributed to the nonlinear data in case of linear kenrel, and to the lack of correlation between inputs and outputs to aim the classification of nearby values. However, for the $DI_{G,PA}$, where all target values are closer to zero, estimation performances are higher for all models compared to ISRT estimation performances which is not property estimated only to the most damaged levels. SVM RBF reveals similar overall classification performance to the RFs, however MSE is greater. It is interesting that all models achieve 100% correct classification rate for $DI_{G,PA}$ to all levels apart of the three more damaged ones (levels 1, 4 and 7). The GA-ANFIS in most levels displays greater MSEs than the rest of the models. GA-ANFIS uses fuzzy logic combined with neural networks and uses a GA to optimize fuzzification level parameters. Since ANNs perform well, the low performance of ANFIS is attributed to fuzzy rules, not being able to effectively relate the parameters with the damage indices.

Figures 5 and Figure 6 illustrate graphically the numerical results of Tables 7 and 8, regarding the MSE, to help visualize and better understand the results. At this point, it is worth mentioning again that MSE is not an objective measure for levels of damage class 4; class 4 refers to the total collapse of the building, regardless of the exact predicted damage index value, thus the value of the MSE. From these figures, it can be seen that ANNs and RFs outperform all other models, especially at the most damaged floors where estimation is more complicated than those with less damage. ANNs display lower MSEs per floor; in most cases. However, average MSE for all floors and correct classification rates, are higher with the RFs.

Comparative results indicate that the two most effective models for damage estimation per floor, are the RFs and ANNs, displaying similar performances. Both succeed minimum MSEs between target and estimated damage values and maximum correct classification rates. ANNs resulted in lower MSEs per floor in most cases, while RFs resulted in higher classification rates per floor in most cases.

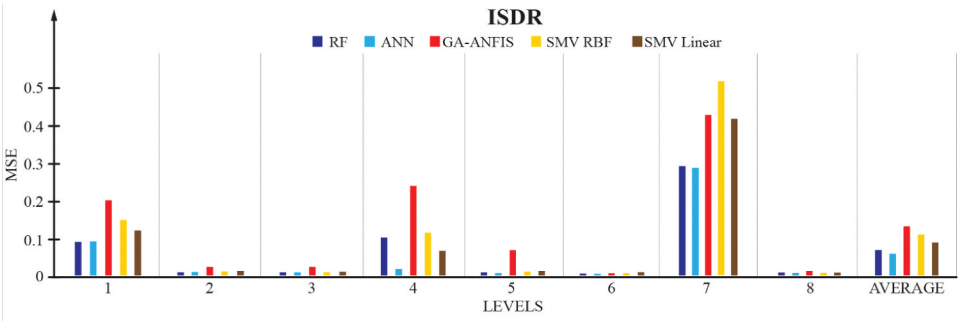

Figure 5. Graphical representation of MSE for ISDR estimation for all models, per level.

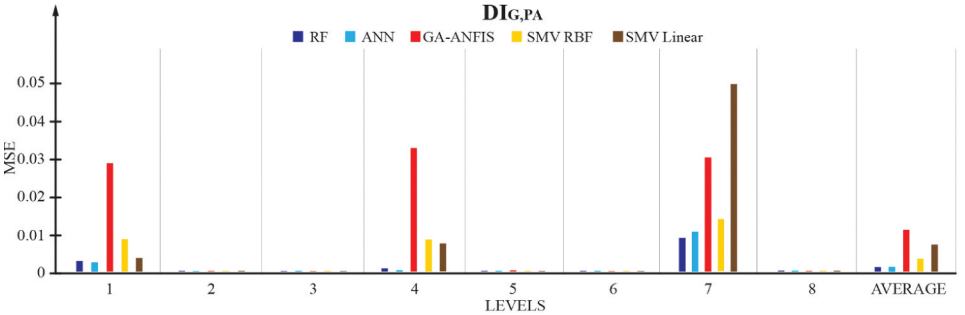

Figure 6. Graphical representation of MSE for $DI_{G,PA}$ estimation for all models, per level.

The proposed method can be extended to different kind of buildings in order to verify the performance of the models or examine additional models in order to conclude to the most robust architecture. Development of an application that all residents of a building could use shortly after an earthquake to get informed about the damage status of the structure and provide instructions depending on the damage estimation on each floor separately, would be a step toward the integration of the methodology in a real-life application for targeted earthquake crisis management.

Further Evaluation

In what follows, the performance of the two models that stand out, RFs and ANNs, is presented throughout the preprocessing steps of data-mining and feature extraction. The objective is to evaluate the preprocessing process by highlighting the induced improvement on the performance of the models that is due to the combination of outlier detection methods and mRMR.

More specifically, the preprocessing includes two main steps: (1) a data-mining process on the seismic accelerograms dataset using a combination of two outlier detection techniques, the isolation forest and the Z-score, toward

Table 11. Preprocessing evaluation results for RFs on ISDR estimation.

	RF					
Levels	**Exp1 (200x18)**		**Exp2 (155x18)**		**Exp3 (155x3)**	
	MSE	**Class. rate**	**MSE**	**Class. rate**	**MSE**	**Class. rate**
Level 1	0.1693	88.16%	0.1497	86.61%	0.0982	83.65%
Level 2	0.0068	95.20%	0.0035	97.04%	0.0052	95.01%
Level 3	0.0032	95.81%	0.0019	95.36%	0.0034	96.31%
Level 4	0.0510	90.20%	0.0345	90.55%	0.1022	93.10%
Level 5	0.0082	90.59%	0.0067	92.10%	0.0085	94.09%
Level 6	0.0035	97.87%	0.0039	96.66%	0.0050	96.23%
Level 7	0.2519	82.23%	0.1504	86.57%	0.2917	86.54%
Level 8	0.0021	89.49%	0.0023	90.40%	0.0027	90.02%
ALL	0.0620	91.19%	0.0441	91.91%	0.0646	91.87%

Table 12. Preprocessing evaluation results for ANNs on ISDR estimation.

	ANN					
Levels	**Exp1 (200x18)**		**Exp2 (155x18)**		**Exp3 (155x3)**	
	MSE	**Class. rate**	**MSE**	**Class. rate**	**MSE**	**Class. rate**
Level 1	0.1726	78.19%	0.2522	68.79%	0.0991	75.85%
Level 2	0.0094	95.92%	0.0046	96.87%	0.0055	95.19%
Level 3	0.0049	96.11%	0.0029	96.07%	0.0021	96.29%
Level 4	0.4960	58.48%	0.0255	93.28%	0.0197	93.95%
Level 5	0.0448	80.29%	0.0095	91.22%	0.0069	95.02%
Level 6	0.0044	97.35%	0.0042	97.00%	0.0047	96.53%
Level 7	**2.1197**	26.55%	**0.1688**	69.38%	0.2878	75.65%
Level 8	0.0030	90.70%	0.0034	92.69%	0.0025	92.20%
ALL	0.3568	77.95%	0.0589	88.16%	0.0535	90.08%

uniform seismic signal data samples and (2) a feature selection algorithm on the extracted seismic parameters from the response signals of the building, mRMR, toward representative features as subsequent inputs to the intelligent models. Thus, the initial dataset was reduced from 200 seismic signals to 155, and the parameters were reduced from 18 to three parameters. Tables 11 and 12 present MSEs and correct classification rates, for the two models, RFs and ANNs.

Both tables include the results, out of three experiments for both damage indices:

- Exp1: initial data set of 200 accelerograms and an initial set of 18 parameters,
- Exp2: reduced data set after outlier detection, of 155 accelerograms and initial set of 18 parameters and finally,
- Exp3: 155 accelerograms and 3 parameters after feature selection algorithm. This is the final selected configuration.

All experiments were executed 100 times, and all numbers on Tables 11 and 12 refer to the average result of all trials. Results indicate the gradual improvement of the performance of both models, as a result of the induced

preprocessing techniques. From the tables, it is obvious that for the ANNs, outlier detection, from Exp1 to Exp2, resulted in major performance improvement, especially in level 7, where MSE reduced from 2.11 to 0.16. Some of the classification results per floor of Exp2 are not improved, however, the average classification rate for all floors is improved.

From Exp2 to Exp3, feature selection further improves the final results. Only on level 4 the MSE is not improved. However, this is not mirrored in the classification accuracy. In the case of the RFs, only the outlier detection results on overall improvement. Feature selection did not further improve the performance.

Conclusions

Fast and accurate determination of the degree of damage on each floor provides crucial information about the post-seismic condition of structures, aiming toward the targeted aim to the primarily affected floors, but also for the subsequent maintenance of the structure.

In this work, five intelligent models were tested for numerical damage estimation and damage potential classification, separately for every floor of an examined building, toward damage estimation, classification and localization. The initial dataset of 200 natural and artificial accelerograms was subjected to a data-mining process using a combination of two outlier detection techniques, the Isolation Forfourst and the Z-score, and it was reduced to 155 seismic signal data samples. Each signal was represented by 18 seismic parameters derived from three response signals of the examined building; displacement, acceleration and velocity response signals. The 18 parameters were subjected to a feature selection algorithm, mRMR, and three parameters resulted as the most correlated with the examined indices and less related among them. The three parameters were the input to five intelligent models, while a damage index value was the output. The proposed method was tested for two global damage indices, ISDR and $DI_{G,PA}$, classifying the structural damage on each floor into 4 discrete categories. All five models were optimized before tested, and objective results were obtained as the average of 100 trials. Results indicated RFs and ANNs as the most effective models for the problem under study, displaying similar performances. RFs reached average correct classification rates for all floors of up to 91.87% for ISDR and of up to 96.87% for $DI_{G,PA}$, with corresponding average MSE values 6.46E-02 and 1.69E-03, respectively. ANNs reached average correct classification rates for all floors, a little less than RFs, of up to 90.12% for ISDR and of up to 96.25% for $DI_{G,PA}$, with corresponding average MSE values 5.35E-02 and 1.73E-03, respectively, but reported lower MSE than RFs in most of the building floors separately. The proposed strategy is generic, and it can be applied to different types of buildings.

ORCID

E. Vrochidou http://orcid.org/0000-0002-0148-8592

References

Aghaeipoor, F., and M. M. Javidi. 2020. A hybrid fuzzy feature selection algorithm for high-dimensional regression problems: An MRMR-based framework. *Expert Systems with Applications* 162 (December):113859. doi:10.1016/j.eswa.2020.113859.

Andreadis, I., I. Tsiftzis, and A. Elenas. 2007. Intelligent seismic acceleration signal processing for damage classification in buildings. *IEEE Transactions on Instrumentation and Measurement* 56 (5):1555–64. doi:10.1109/TIM.2007.895620.

Arias, A. 1970. A measure of earthquake intensity. Seismic Design for Nuclear Power Plants.

Begic Fazlic, L., K. Avdagic, and S. Omanovic. 2015. GA-ANFIS expert system prototype for prediction of dermatological diseases. *Studies in Health Technology and Informatics* 210:622–26. doi:10.3233/978-1-61499-512-8-622.

Berkley University of California. 2020. Pacific earthquake engineering research center (PEER) strong ground motion databases. Accessed November 23. https://peer.berkeley.edu/peer-strong-ground-motion-databases .

Cherkassky, V., and Y. Ma. 2004. Practical selection of SVM parameters and noise estimation for SVM regression. *Neural Networks* 17 (1):113–26. doi:10.1016/S0893-6080(03)00169-2.

Downey, A., A. D'Alessandro, F. Ubertini, and S. Laflamme. 2018. Automated crack detection in conductive smart-concrete structures using a resistor mesh model. *Measurement Science and Technology* 29 (3):035107. doi:10.1088/1361-6501/aa9fb8.

Elenas, A., and K. Meskouris. 2001. Correlation study between seismic acceleration parameters and damage indices of structures. *Engineering Structures* 23 (6):698–704. doi:10.1016/S0141-0296(00)00074-2.

Elenas, A., E. Vrochidou, P. Alvanitopoulos, and I. Andreadis. 2013. Classification of seismic damages in buildings using fuzzy logic procedures. *Computational Methods in Applied Sciences* 335–44. doi:10.1007/978-94-007-5134-7_20.

Ferreira, T. M., N. Mendes, and R. Silva. 2019. Multiscale seismic vulnerability assessment and retrofit of existing masonry buildings. *Buildings* 9 (4):91. doi:10.3390/buildings9040091.

Ghobarah, A., H. Abou-Elfath, and A. Biddah. 1999. Response-based damage assessment of structures. *Earthquake Engineering & Structural Dynamics* 28 (1):79–104. doi:10.1002/(SICI)1096-9845(199901)28:1<79::AID-EQE805>3.0.CO;2-J.

Hait, P., A. Sil, and S. Choudhury. 2020. Seismic damage assessment and prediction using artificial neural network of RC building considering irregularities. *Journal of Structural Integrity and Maintenance* 5 (1):51–69. doi:10.1080/24705314.2019.1692167.

Hornik, K. 1991. Approximation capabilities of multilayer feedforward networks. *Neural Networks* 4 (2):251–57. doi:10.1016/0893-6080(91)90009-T.

Huang, C. S., S. L. Hung, C. M. Wen, and T. T. Tu. 2003. A neural network approach for structural identification and diagnosis of a building from seismic response data. *Earthquake Engineering & Structural Dynamics* 32 (2):187–206. doi:10.1002/eqe.219.

Huang, Q., J. Mao, and Y. Liu. 2012. An Improved Grid Search Algorithm of SVR Parameters Optimization. 2012 IEEE 14th International Conference on Communication Technology, 1022–26. IEEE. doi:10.1109/ICCT.2012.6511415.

Husid, R. 1969. Características de Terremotos. Análisis General. *Revista IDIEM* 8 (1):21–42.

Kappos, A. J. 2016. An overview of the development of the hybrid method for seismic vulnerability assessment of buildings. *Structure and Infrastructure Engineering* 12 (12):1573–84. doi:10.1080/15732479.2016.1151448.

Kubo, T., Y. Hisada, M. Murakami, F. Kosuge, and K. Hamano. 2011. Application of an earthquake early warning system and a real-time strong motion monitoring system in emergency response in a high-rise building. *Soil Dynamics and Earthquake Engineering* 31 (2):231–39. doi:10.1016/j.soildyn.2010.07.009.

Lei, X., L. Sun, Y. Xia, and T. He. 2020. Vibration-based seismic damage states evaluation for regional concrete beam bridges using random forest method. *Sustainability* 12 (12):5106. doi:10.3390/su12125106.

Lin, K. Y., and T. K. Lin. 2020. Real-time seismic structural response prediction system based on support vector machine. *Earthquakes and Structures* 18 (2):163–70. doi:10.12989/eas.2020.18.2.163.

Liu, F. T., K. M. Ting, and Z.-H. Zhou. 2008. Isolation forest. 2008 Eighth IEEE International Conference on Data Mining, 413–22. IEEE. doi:10.1109/ICDM.2008.17.

Masri, S. F., A. W. Smyth, A. G. Chassiakos, T. K. Caughey, and N. F. Hunter. 2000. Application of neural networks for detection of changes in nonlinear systems. *Journal of Engineering Mechanics* 126 (7):666–76. doi:10.1061/(ASCE)0733-9399(2000)126:7(666).

Morfidis, K., and K. Kostinakis. 2017. Seismic parameters' combinations for the optimum prediction of the damage state of R/C buildings using neural networks. *Advances in Engineering Software* 106 (April):1–16. doi:10.1016/j.advengsoft.2017.01.001.

Morfidis, K., and K. Kostinakis. 2018. Approaches to the rapid seismic damage prediction of r/c buildings using artificial neural networks. *Engineering Structures* 165 (June):120–41. doi:10.1016/j.engstruct.2018.03.028.

Morfidis, K., and K. Kostinakis. 2019. Comparative evaluation of MFP and RBF neural networks' ability for instant estimation of r/c buildings' seismic damage level. *Engineering Structures* 197 (October):109436. doi:10.1016/j.engstruct.2019.109436.

Nguyen, M. H., and F. de la Torre. 2010. Optimal feature selection for support vector machines. *Pattern Recognition* 43 (3):584–91. doi:10.1016/j.patcog.2009.09.003.

Park, Y., and A. H. -. S. Ang. 1985. Mechanistic seismic damage model for reinforced concrete. *Journal of Structural Engineering* 111 (4):722–39. doi:10.1061/(ASCE)0733-9445(1985)111:4(722).

Perrault, M., and P. Guéguen. 2015. Correlation between ground motion and building response using california earthquake records. *Earthquake Spectra* 31 (4):2027–46. doi:10.1193/062413EQS168M.

Rousseeuw, P. J., and M. Hubert. 2011. Robust statistics for outlier detection. *WIREs Data Mining and Knowledge Discovery* 1 (1):73–79. doi:10.1002/widm.2.

Rus, K., V. Kilar, and D. Koren. 2018. Resilience assessment of complex urban systems to natural disasters: A new literature review. *International Journal of Disaster Risk Reduction* 31 (October):311–30. doi:10.1016/j.ijdrr.2018.05.015.

Trifunac, M. D., and A. G. Brady. 1978. A study on the duration of strong earthquake ground motion. *Bulletin of the Seismological Society of America* 65 (3):581–626.

Tsiftzis, I., I. Andreadis, and A. Elenas. 2006. Fuzzy system for seismic signal classification. *IEE Proceedings - Vision, Image, and Signal Processing* 153 (2):109–14. doi:10.1049/ip-vis:20050068.

Vrochidou, E., P. F. Alvanitopoulos, I. Andreadis, A. Elenas, and K. Mallousi. 2014. Synthesis of artificial spectrum-compatible seismic accelerograms. *Measurement Science and Technology* 25 (8):085002. doi:10.1088/0957-0233/25/8/085002.

Vrochidou, E., P. F. Alvanitopoulos, I. Andreadis, and A. Elenas. 2016. Structural damage estimation in mid-rise reinforced concrete structure based on time–frequency analysis of

seismic accelerograms. *IET Science, Measurement & Technology* 10 (8):900–09. doi:10.1049/iet-smt.2016.0129.

Vrochidou, E., P.-F. Alvanitopoulos, I. Andreadis, and A. Elenas. 2018. Intelligent systems for structural damage assessment. *Journal of Intelligent Systems* 29 (1):378–92. doi:10.1515/jisys-2017-0193.

Yang, D., J. Pan, and G. Li. 2010. Interstory drift ratio of building structures subjected to near-fault ground motions based on generalized drift spectral analysis. *Soil Dynamics and Earthquake Engineering* 30 (11):1182–97. doi:10.1016/j.soildyn.2010.04.026.